Improving confidence in crystal structure solutions using NMR crystallography: the case of β-piroxicam

Andrew S. Tatton[a], Helen Blade[b], Steven P. Brown[c], Paul Hodgkinson[d], Leslie P. Hughes[b], Sten Nilsson Lill[e], and Jonathan R. Yates[a]

[a] Department of Materials, University of Oxford, Oxford, OX1 3PH, UK

E-mail: Andrew.Tatton@materials.ox.ac.uk, Jonathan.Yates@materials.ox.ac.uk

[b] Pharmaceutical Development, AstraZeneca, Macclesfield, SK10 2NA, UK

E-mail: Les.Hughes2@astrazeneca.com

[c] Department of Physics, University of Warwick, Coventry, CV4 7AL, UK

E-mail: S.P.Brown@warwick.ac.uk

[d] Department of Chemistry, Durham University, Durham, DH1 3LE, UK

E-mail: Paul.Hodgkinson@durham.ac.uk

[e] Early Product Development, Pharmaceutical Sciences, IMED Biotech Unit, AstraZeneca Gothenburg, Mölndal, SE-431 83, Sweden

Abstract

NMR crystallographic techniques are used to validate a structure of β-piroxicam determined from powder X-ray diffraction (PXRD) with a relatively poor R-factor. Geometry optimisation of PXRD- and single-crystal XRD- derived structures results in convergence to the same energy of the structures, with minimal atomic displacements, and good agreement of gauge-included projector augmented wave (GIPAW) calculated and experimentally determined NMR ^{1}H, ^{13}C and ^{15}N chemical shifts and ^{14}N quadrupolar parameters. Calculations on isolated molecules combined with 2D magic-angle spinning (MAS) ^{1}H double-quantum (DQ) and ^{14}N-^{1}H NMR experiments confirm the 3D packing arrangement of β-piroxicam. NMR crystallography is shown to be an effective means of validating crystal structures that might otherwise be considered sceptically on the basis of diffraction data alone.

Introduction

A comprehensive understanding of the different crystal structures adopted by an active pharmaceutical ingredient (API) is critical throughout the development process of a new medicine for both characterisation

and regulatory purposes. A detailed knowledge of the specific crystal structures facilitates an improved understanding of the polymorph landscape, reliable property predictions, both physical and chemical, and the ability to perform better solid-state risk assessments.[1] In a pharmaceutical context, a solid-state risk assessment is performed to aid in selection of the final commercial solid form and manufacturing control required.

Structural elucidation of a material using single crystal X-ray diffraction (SCXRD) is typically the preferred structure solution technique, but growth of a single crystal of sufficient size and quality for SCXRD is often not possible, and alternative methods must be considered. PXRD remains a more challenging, although increasingly feasible,[2] pathway for obtaining a structure solution relative to SCXRD. For example, light elements, such as hydrogen, have a low electron density and therefore interact only weakly with X-ray radiation. This is a limitation where accurate determination of a hydrogen position is crucial, for example when distinguishing between a pharmaceutical salt or co-crystal.

A structural model from a diffraction study is accompanied by a discrepancy value, which quantifies the fit of the proposed structural model to experimental data. Although a number of discrepancy values have been presented and discussed,[3-5] the mostly widely used is the conventional R-factor,[6] which describes agreement between the amplitude of structure factors determined from the proposed structural model and corresponding experimental X-ray diffraction data. The R-factor is an important indicator of the confidence of a crystal structure model, but it is important to note that a low R-factor does not always correspond to a good crystal structure description.[7] There is no single source of a high R-factor, rather a multitude of potential uncertainties exist. These can include high-temperature acquisition, a small number of sampling angles, low quality data (weak intensity, poor resolution) and somewhat paradoxically, higher quality data (increased intensity and/or resolution) that may amplify the influence of any systematic errors.[5] In the case where a structural model is solved with a high R-factor, or a degree of uncertainty in the structural model exists, then a methodology that complements the diffraction data to increase confidence in the structural model is highly desirable.

In recent years, NMR crystallography,[8-14] which utilises a combination of solid-state NMR experimental data and calculated NMR parameters, has emerged as a powerful tool for structural refinement and elucidation of various materials, such as pharmaceutical salts,[15-16] co-crystals,[17-20] and hydrates.[16, 21-22] Furthermore, the wide range of NMR-active nuclei potentially included within a NMR crystallography study increases the range of systems that can be studied. The accuracy of a proposed model can be gauged from a comparison between chemical shift values,[23-24] and for spin >½ nuclei, the quadrupolar interaction can also be determined, using experiment and calculation.[25-27] Insight into intermolecular packing configurations can be provided by 2D correlation experiments, where an observed correlation between atoms is due to through-space or through-bond couplings. Experimentally observed interactions between atoms in neighbouring molecules can then be compared to the expected intermolecular configuration from a geometry-optimised structural model.[28] NMR crystallography has also been used extensively to probe intermolecular interactions that determine the 3D packing arrangement, such as hydrogen bonding and aromatic dispersive forces.[29-31] Quantitative analysis of intermolecular interactions has been demonstrated from comparison between calculated chemical shift values obtained from a full crystal calculation relative to chemical shifts of an isolated molecule.[32]

To demonstrate that NMR crystallography can act as a complementary methodology for diffraction studies to increase the confidence in a structural model, we present an NMR crystallography study for different structural models of piroxicam, with emphasis upon a structural model solved from PXRD with a high R-factor. Piroxicam (IUPAC name: 4-hydroxy-2-methyl-*N*-(2-pyridinyl)-2*H*-1,2-benzothiazine-3-carboxamide-1,1-dioxide) is a non-steroidal, analgesic, anti-inflammatory drug.[33] Piroxicam does exhibit polymorphism, although only β-piroxicam, which is also referred to as form I by Sheth et al.,[34] is discussed within this article. Recently, Shi et al.[35] deposited a β-piroxicam structure in the CSD solved from SCXRD (CSD reference code: BIYSEH13), with an associated R-factor of 2.4%. Previously β-piroxicam has been solved from PXRD (CSD reference code: BIYSEH03) with a reported R-factor of 19%.[36] These particular values may imply that the former model is a significantly more accurate structure solution than the latter,

and is explored in this work. Note that the cause of the high R-factor for BIYSEH03 is not discussed by Sheth et al.[36]

These two structures provide an ideal case study owing to their different R-factors and respective methodologies used to solve the structure. Initially, the structural models (BIYSEH03 and BIYSEH13) are geometry optimised by applying Density Functional Theory (DFT) using the CASTEP code.[37] Using the geometry-optimised structures, NMR parameters are calculated using the GIPAW (gauge-including projector augmented wave) method.[38-39] 1D and 2D magic-angle spinning (MAS) solid-state NMR experiments are performed to determine ^{1}H, ^{13}C and ^{15}N chemical shifts for comparison to calculated NMR chemical parameters derived from the geometry optimised structural model. Additionally interatomic distances from the geometry-optimised structural model are linked to experimental data from 2D MAS NMR correlation experiments.

Experimental and calculation details

β-piroxicam was purchased from Sigma Aldrich and was used as supplied. PXRD confirmed that correct form I was supplied (see supporting information, Fig. S1). ^{13}C ramped cross-polarisation magic-angle spinning (CPMAS)[40] and 2D ^{13}C-^{1}H CP Heteronuclear Correlation (HETCOR)[41] solid-state NMR experiments were performed using a Bruker Avance III HD spectrometer operating at a ^{1}H Larmor frequency of 399.9 MHz using a Bruker 4 mm double resonance probe at spinning frequencies of 12.5 kHz and 10 kHz, respectively. For ^{1}H-^{13}C cross-polarisation, SPINAL-64[42-43] ^{1}H decoupling was applied during acquisition at a nutation frequency of 100 kHz for 35 ms. The ^{1}H 90° pulse duration was 2.5 μs, and ^{13}C magnetisation was created using a CP ramp of magnitude 90% to 100% for a duration of 2 ms. A recycle delay of 10 s was used, and a total of 1024 transients were co-added. During ^{13}C-^{1}H 2D HETCOR experiments, SPINAL-64 ^{1}H decoupling was applied during t_2 at a nutation frequency of 100 kHz for a duration of 20 ms, and ^{1}H homonuclear decoupling during t_1 was achieved using the Frequency Switched Lee-Goldburg (FSLG)[44] method at a nutation frequency of 100 kHz. A total of 38 t_1 FIDs were recorded at increments of 75.53 μs using the States-TPPI method for sign discrimination in the indirect dimension. A

recycle delay of 5 s was used, and 320 transients were co-added for each slice. ^{1}H-^{13}C magnetisation transfer was achieved using a magnitude 50% to 100% ramp applied on the proton channel. ^{13}C chemical shifts are referenced to TMS at 0 ppm, using the CH_2 peak in adamantane at 38.5 ppm as a secondary reference.[45]

^{1}H experiments were performed using a Bruker Avance III HD spectrometer operating at a ^{1}H Larmor frequency of 399.9 MHz using a Bruker 1.3 mm double resonance probe. Single pulse experiments were performed using a spinning frequency of 65 kHz, 8 co-added transients and a recycle delay of 30 s. ^{1}H DQ-SQ Back-to-Back (BABA)[46-47] rotor synchronised (in F_1) spectra were obtained using a spinning frequency of 60 kHz, 16 co-added transients per each t_1 slice and a recycle delay of 30 s. ^{1}H chemical shifts are referenced to TMS at 0 ppm, using the CH_2 peak in adamantane at 1.8 ppm as a secondary reference.[48]

^{15}N cross-polarisation experiments were performed using a Bruker Avance II spectrometer operating at a ^{1}H Larmor frequency of 500.5 MHz and a Bruker 4 mm double resonance probe at a spinning frequency of 10 kHz. SPINAL-64 ^{1}H decoupling was applied during acquisition at a nutation frequency of 100 kHz for 40 ms. The ^{1}H 90° pulse duration was 2.5 μs, and ^{15}N magnetisation was created using a CP ramp of magnitude 50% to 100% for a duration of 5 ms. A total of 7168 co-added transients were acquired using a recycle delay of 10 s. ^{15}N chemical shifts are referenced to liquid nitromethane at 0 ppm,[49] using the NH_3^+ peak in glycine at −346.9 ppm as a secondary reference. To convert to the chemical shift scale frequently used in protein NMR, where the alternative IUPAC reference (see Appendix 1 of Ref. 50) is liquid ammonia at 50 °C, it is necessary to add 379.5 ppm to the given values.[51]

^{14}N-^{1}H Heteronuclear Multiple Quantum (HMQC) experiments[52] were performed using a Bruker Avance III spectrometer operating at a ^{1}H Larmor frequency of 700.1 MHz using a Bruker 1.3 mm triple resonance probe, operating in double resonance mode, at a spinning frequency of 60 kHz. Rotary resonance recoupling (R^3) with a n=2 resonance condition[53] with an x $-x$ phase inversion[54-55] of individual blocks lengths of duration 16.7 μs was implemented. A total of 16 and 32 co-added transients were acquired for shorter and longer recoupling time experiments, respectively, and a recycle delay of 32 s was used. States-TPPI was

used to provide sign discrimination, and a total of 52 t_1 FIDs were recorded at increments of 16.7 μs. ^{14}N shifts are referenced to liquid nitromethane at 0 ppm, using the NH_4 peak in a saturated aqueous solution of NH_4Cl at −352.9 ppm as a secondary reference (see Table 2 of Ref. 49).

First-principle calculations were performed using CASTEP[37] version 17.0.8 in the Materials Studio platform. All calculations employed the Perdew-Burke-Ernzerhorf (PBE)[56] functional with the Tkatchenko and Scheffler (TS) dispersion scheme,[57] and on-the-fly generated ultrasoft pseudopotentials (OTFG). For all geometry optimisation calculations, a plane-wave cut-off energy of 600 eV was used with a Monkhurst-Pack grid with a minimum k-point sampling space of 0.05 $Å^{-1}$, which corresponds to a k-point grid with dimensions (3, 1, 1). Crystal structures of BIYSEH03 and BIYSEH13 were downloaded from the Cambridge Structural Database. Note that the lattice parameters stated for BIYSEH03 in Table 1 of Ref. 36 differ slightly from those of the deposited structure. All 144 atoms in the unit cell ($Z = 4$, $Z' = 1$) were allowed to relax, unless otherwise stated, and calculations were performed with unit cell parameters fixed, unless otherwise stated. Distances and angles presented are for geometry-optimised structures. The space group $P2_1/c$ was preserved during all relaxations. NMR shielding values were calculated using the GIPAW[38-39] method for the geometry optimised structures, with a plane-wave cut-off energy of 700 eV, and the same k-point grid and pseudopotentials as for the relaxations. Visualisation of GIPAW NMR results was performed using MagresView.[58]

Results and Discussion

Effect of geometry optimisation on different β-piroxicam structure solutions

The chemical structure of β-piroxicam is shown with numbering in Fig. 1a. Different numbering schemes for piroxicam are found in the literature.[35, 59-61] The carbon atom labels in Fig. 1a agree with those used in Sheth et al.[59] The hydrogen atoms take the number of their respective through-bond heteroatom (methyl protons are labelled H10a, H10b, and H10c).

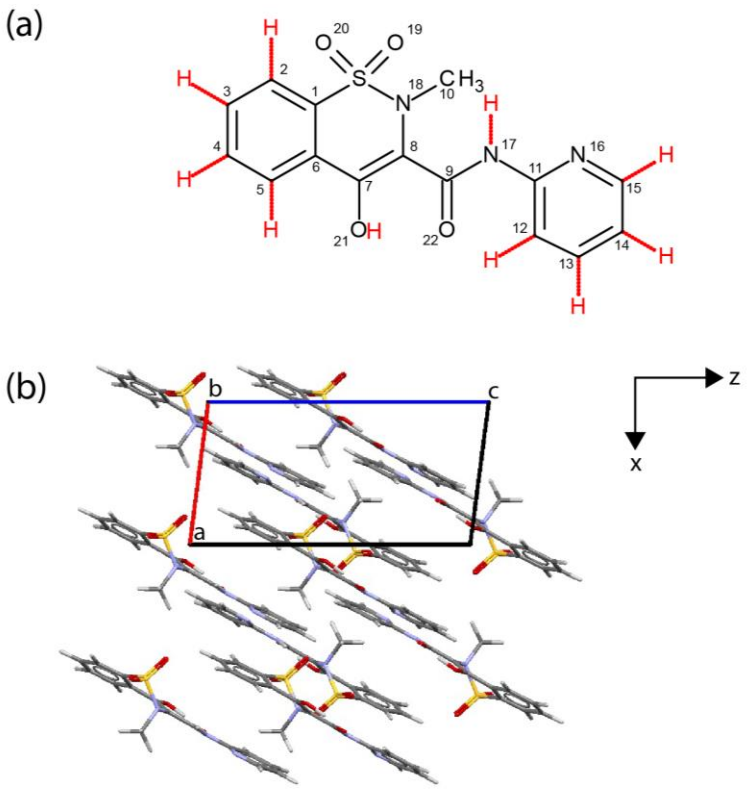

Figure 1. (a) Chemical structure of β-piroxicam. (b) View along crystallographic axis b showing the stacking arrangement in the BIYSEH03 structure.

Both the β-piroxicam structures studied are modelled in the monoclinic space group $P2_1/c$, one molecule per asymmetric unit cell ($Z' = 1$) and four molecules in the conventional unit cell ($Z = 4$). Inspection of both β-piroxicam structural models indicate a short distance between N17 and O19 that suggests a putative intermolecular N17-H17…O19 hydrogen bond, which may direct the formation of dimers along the crystallographic axis b, as suggested in previous studies.[34, 61-62] Intramolecular hydrogen bonding has also been indicated between N17-H17…N18[34] and O21-H21…O22.[60-61]

Visualisations of the structural models, before and after geometry optimisation (unit cell parameters fixed, all atoms optimised), are presented in Fig. 2a and Fig. 2b, respectively. After geometry optimisation, there is a lengthening of heteronuclear X-H bond lengths for both structural models, and, for BIYSEH03 only, a slight rotation of the pyridine ring and a change in direction of the NH bond. The displacement in atomic

position of each proton and carbon due to geometry optimisation is presented in the supporting information (Tables S1-S3).

In Fig. 2c, an additional BIYSEH03 structural overlay is included, shown in green, obtained from a geometry optimisation where only hydrogen positions were allowed to relax. It is evident that allowing only hydrogen positions to relax prohibits the rotation of the pyridine ring, since the carbon atoms are fixed. Furthermore, the direction of the N17-H17 bond angle is now located at an intermediate point between the original, non-geometry-optimised structure, and the all-atom geometry-optimised structure. This indicates that the structure solution from PXRD did not locate N17 at its lowest energy position, and as can be seen in Table S2, the largest distance between hydrogen positions between fully and partially (hydrogen only) geometry optimised structures is for H17.

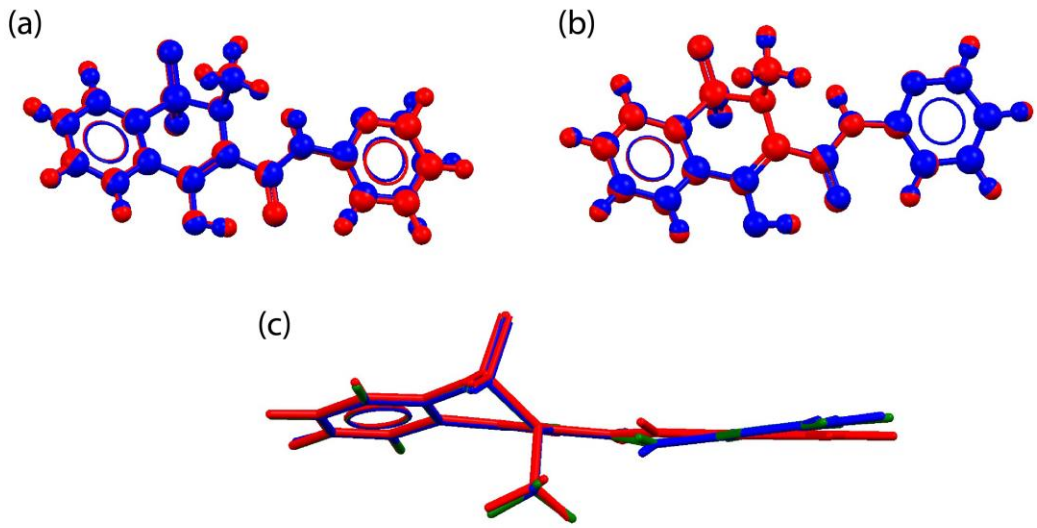

Figure 2. Ball and stick representations before (blue) and after (red) geometry optimisation, of (a) BIYSEH03 and (b) BIYSEH13. Unit cell parameters were fixed during geometry optimisation. (c) Overlay of BIYSEH03 before geometry optimisation (blue), geometry optimisation of proton positions only (green) and full-atom geometry-optimisation (red).

Table 1. Selected output parameters from all atom geometry optimisations for BIYSEH03 and BIYSEH13, with and without relaxation of unit cell parameters.

Structure code	Unit cell parameters	RMSD displacement [a] / Å		Lattice parameters				Volume
		H	C	*a* / Å	*b* / Å	*c* / Å	β / ° [c]	*V* / Å^3

BIYSEH03	Fixed	0.036	0.015	7.16	15.18	13.99	97.4	1504.5
BIYSEH03	Relaxed [b]	0.033	0.016	7.07	15.41	13.75	95.3	1492.4
BIYSEH13	Fixed [b]	0.010	0.005	7.03	14.98	13.89	96.4	1453.5
BIYSEH13	Relaxed	0.009	0.006	7.05	15.31	13.84	95.7	1486.7

[a] Displacement relative to non-geometry optimised structural model, determined as an average of the displacement in atomic co-ordinates of the respective nuclei within 1 molecule. [b] Starting unit cell parameters were the same as those for the respective geometry optimisation with fixed unit cell parameters. [c] Symmetry group $P2_1/c$ was preserved, therefore $\alpha = \gamma = 90°$ was maintained.

As shown in Table 1, it is evident that there is a significantly larger shift in atomic positions, reflected in the RMSD values, after a geometry optimisation for the crystal structure derived from PXRD. This structure was solved using DASH,[63] which by default does not include the hydrogen atoms in the structure factor calculation, and hydrogen atoms are simply added at standard distances.[36] For the structure solution of BIYSEH13 determined from SCXRD, the electron density difference map has been used to assign the hydrogen positions.[35]

Allowing the unit cell parameters to relax during geometry optimisation does not have a significant effect upon the atomic positions relative to the geometry-optimised structure with unit cell parameters fixed, although unit cell parameters and cell volume differ when relaxation of the unit cell parameters is permitted. After unit cell varying optimisation, the energies are the same (less than 0.1 kJ/ mol difference), whereas, with unit cells fixed, one energy is 4.8 kJ / mol lower in energy. Predicted PXRD patterns for the original structural models and subsequent geometry-optimised structures included in Table 1 can be found in the supporting information (Fig. S2). Unsurprisingly, there is a larger difference between predicted powder patterns of BIYSEH03, before and after geometry optimisation, relative to BIYSEH13. After a full atom geometry optimisation, the RMSD value between atomic positions relative to the SCXRD structure solution is 0.19 Å when considered over 15 molecules, which is the default molecular cluster size when comparing crystal packing when using Mercury.

Conversion to an alternate polymorphic form is unlikely as geometry optimisation is always a refinement to a local energy minimum, and therefore will only occur if the starting structure is closer to another form.

In the case of β-piroxicam, no significant change is noted between final structures determined using a geometry optimisation with unit cell parameters allowed to relax, and full atom relaxation, relative to fixed unit cell parameters and protons only allowed to relax during geometry optimisation.

The convergence of the two structures indicates that BIYSEH03, which owing to a high R-factor would normally be treated with a degree of caution in a solid-state risk assessment, is a reasonably sound structural model. Unit cell parameters are slightly different between the two structures, which will account for some of this difference. An overlay of the respective unit cells is included in the Supporting Information (Fig. S3). Note, that these are after a full atom geometry optimisation, with fixed unit cell parameters. Without access to the original diffraction datasets any possible reduction in R-factor from the optimised structure of BIYSEH03 is not determinable.

Comparison between experimental and GIPAW calculated NMR chemical shift values

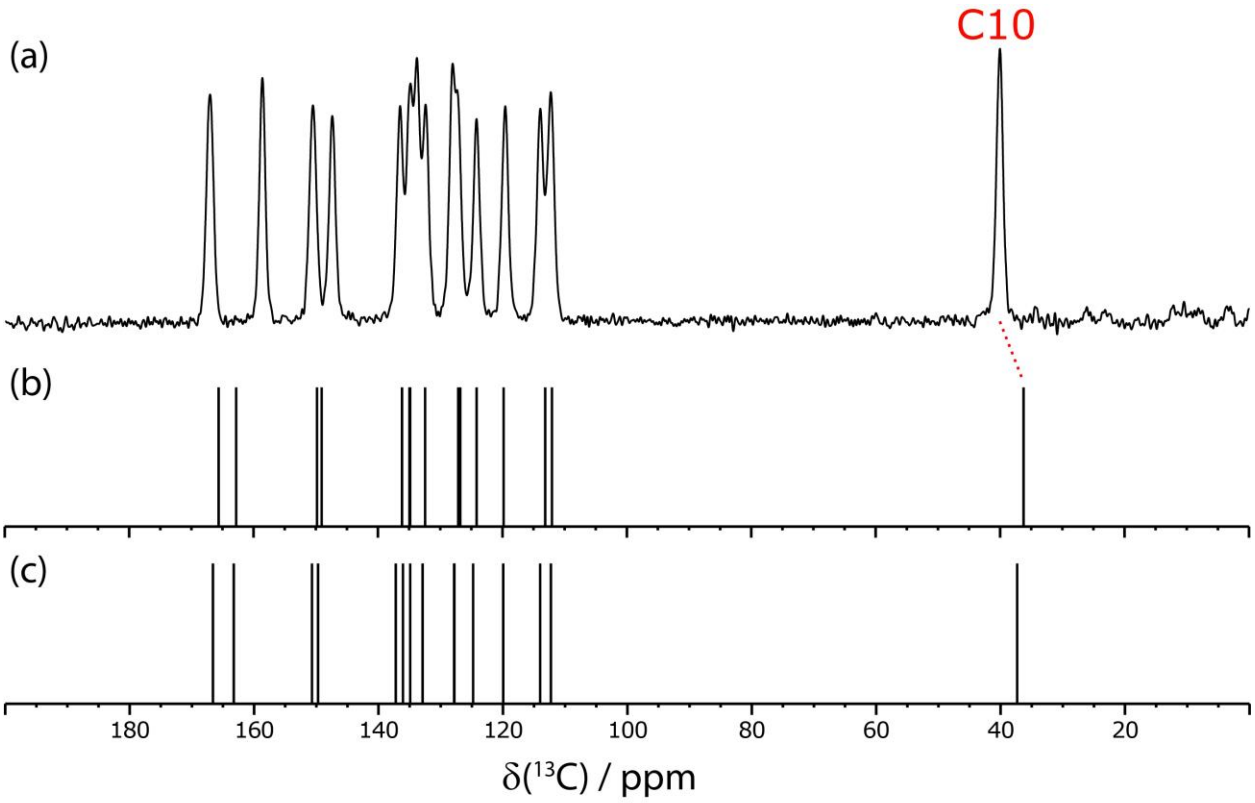

Figure 3. (a) A ^{13}C CPMAS spectrum of β-piroxicam obtained at 9.4 T and a MAS frequency of 12.5 kHz. Stick spectra representing ^{13}C chemical shift GIPAW NMR values calculated for the (b) BIYSEH03 and (c) BIYSEH13 geometry-optimised structures. To convert to a scale comparable to TMS = 0 ppm, $\delta_{iso} = -(\sigma_{iso} - \sigma_{ref})$, where σ_{ref} = 170.4 ppm (b) and 170.2 ppm (c). σ_{ref} was calculated from averaging the $\delta(^{13}C)_{expt}$ and σ_{iso} values.

Particularly if the only structure solution available for a solid-state risk assessment is from PXRD with a high R-factor, then it remains desirable to verify a structure solution with a methodology that is not diffraction based, ideally with a direct link to experiment, NMR crystallography can provide this additional confidence. Furthermore, the RMSD displacement range of the carbon atoms falls below the 0.25 Å limit suggested by van de Streek et al. as an incorrect structure or revealing of interesting structural features,[64] and therefore there is an incentive to investigate if NMR crystallography is sensitive to any finer structural differences.

Figure 3 compares (a) ^{13}C experimental isotropic chemical shift values, determined from a ^{13}C CPMAS experiment, and (b, c) chemical shift values determined from a GIPAW NMR calculation for BIYSEH03 and BIYSEH13, respectively, after geometry optimisation of all atomic positions and fixed unit cell parameters. Experimental assignment was assisted by performing a ^{13}C non-quaternary suppression experiment (see Supporting information, Fig. S4), and is in agreement with previous ^{13}C solid-state NMR studies of piroxicam.[65-67] Previous studies indicate that the associated error in the ^{13}C chemical shift for a GIPAW NMR calculation using the PBE functional is approximately 2 ppm, i.e., approximately 1% of the chemical shift range.[12] Broad agreement is noted between all sites (complete chemical shift tables can be found in the Supporting information, Tables S5-S6) except for C10, as indicated by the red dashed line included in Fig. 3. The RMSD values between experiment and calculated ^{13}C chemical shifts are 1.7 ppm (BIYSEH03) and 1.6 ppm (BIYSEH13), however if C10 is discounted the ^{13}C RMSD value is 1.3 ppm for both models.

The discrepancy in C10 chemical shifts is most likely a consequence of the referencing system used for GIPAW NMR calculation. The challenges in overcoming such a referencing discrepancy are discussed in the supporting information. Additionally, the influence of nuclear delocalisation in methyl proton positions, and their subsequent effect upon the ^{13}C chemical shift,[68] may account for this discrepancy between

experiment and calculation. An alternative approach for the referencing system is to calculate an averaged value of σ_{ref} for a series of well assigned materials,[69-70] or for a single well defined reference compound,[71-72] and apply this value to all further calculations. This approach was not chosen herein as β-piroxicam is a highly aromatic compound, and therefore as discussed by Webber et al.,[73] ^{13}C σ_{ref} values are likely to be skewed by the absence of peaks in the lower ppm ^{13}C region.

As shown in Fig. 2c, a geometry optimisation of BIYSEH03 with only hydrogen positions allowed to relax prevents rotation of the pyridine ring as compared to the case of a full atom geometry optimisation. However, the effect upon ^{13}C GIPAW calculated chemical shieldings is less clear. The ^{13}C magnetic shieldings (σ_{iso}) for BIYSEH03 structures (proton only relaxation versus all atom relaxation) differ by an average of 2.7 ppm. This also influences, however, the determined value of σ_{ref}, which is used to convert magnetic shieldings to a scale comparable to experimental chemical shift values. Consequently, the calculated δ_{iso} values are converted to values that closely match geometry-optimisation conditions. By comparison, the average difference between ^{13}C σ_{iso} values for the BIYSEH13 geometry-optimised structures is 0.7 ppm. This observation is unsurprising, given that the atomic coordinates of BIYSEH13 move less after geometry optimisation.

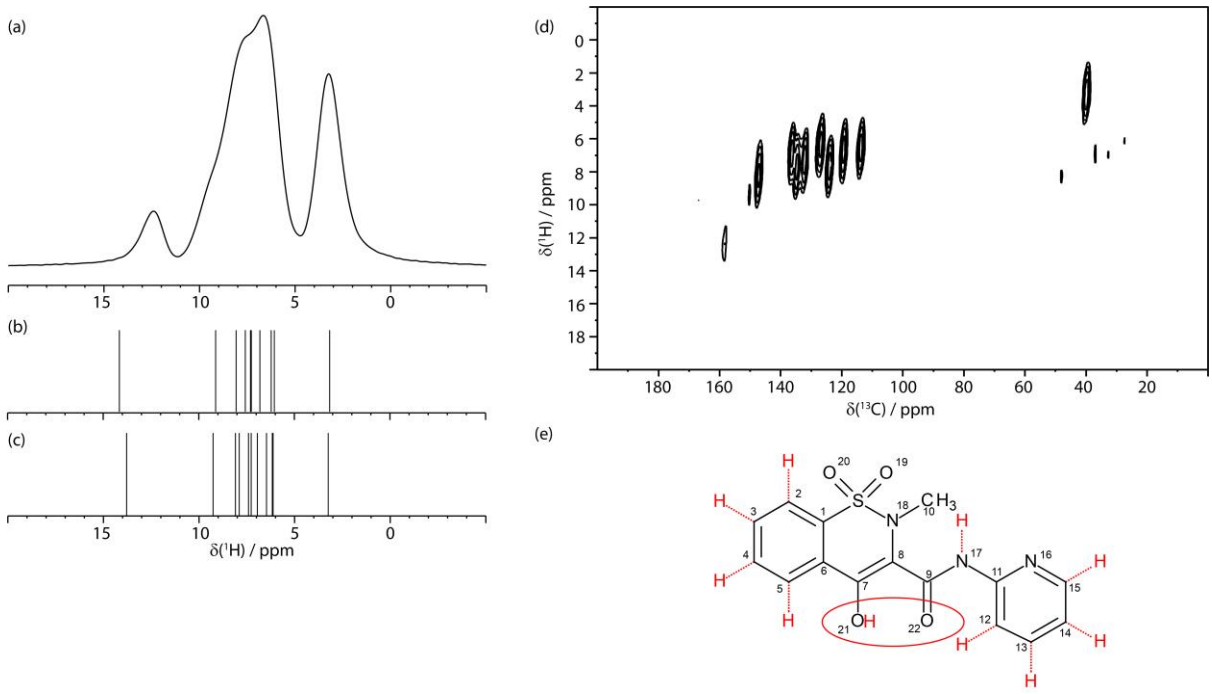

Figure 4. (a) A ^{1}H one pulse spectrum obtained for β-piroxicam at 9.4 T and a MAS frequency of 65 kHz. (b, c) Stick spectra representing ^{1}H chemical shift GIPAW NMR values calculated for the (b) BIYSEH03 and (c) BIYSEH13 geometry-optimised crystal structures. To convert to a scale comparable to TMS = 0 ppm, $\delta_{iso} = -(\sigma_{iso} - \sigma_{ref})$, where σ_{ref} = 30.7 ppm for both structures. σ_{ref} was calculated from averaging the $\delta(^{1}H)_{expt}$ and σ_{iso} values. (d) A ^{13}C-^{1}H HETCOR (ν_r = 10 kHz, B_0 = 9.4 T) spectrum obtained for β-piroxicam using a cross-polarization contact time of 200 μs and FSLG homonuclear decoupling in F_1. (e) Chemical structure of β-piroxicam with intramolecular O21-H21…O22 hydrogen bonding motif highlighted.

As protons often directly participate in the intermolecular packing arrangement, for example via hydrogen bonding or aromatic dispersive forces, any inaccuracies in the structural model will be clearly seen as discrepancies between experimental and calculated GIPAW NMR ^{1}H chemical shift values. Figure 4, parts (a–c), show a comparison between a single-pulse ^{1}H spectrum obtained using fast MAS and stick spectra corresponding to calculated GIPAW NMR chemical shifts of BIYSEH03 and BIYSEH13, respectively. Owing to the presence of strong homonuclear dipolar couplings, ^{1}H solid-state NMR spectra usually yield broad peaks that prevent individual identification of each individual ^{1}H chemical shift. Modest improvement in resolution can be achieved by applying fast MAS; here a MAS rotation frequency of 65 kHz was applied and consequently spectral regions (methyl, aromatic, carboxylic acid), although not individual peaks, are distinguishable. The peaks at approximately 12 and 3 ppm correspond to the carboxylic acid proton and the methyl protons, respectively. However, owing to the large number of

aromatic protons present in piroxicam, it is not possible to individually assign aromatic protons in the region between 5 and 10 ppm using the 1D MAS NMR spectrum.

Individual proton chemical shifts can be identified indirectly using 2D NMR experiments, where the introduction of an indirect dimension allows for improved spectral separation of protons via the heteronucleus. In this case the higher resolution in the ^{13}C dimension is used to indirectly probe proton environments using a ^{13}C-^{1}H HETCOR experiment,[41] which is typically performed at more modest spinning rates so as not to inhibit magnetisation transfer between ^{13}C and ^{1}H nuclei. Improvement of the resolution in the proton dimension can be achieved by application of homonuclear ^{1}H dipolar decoupling (FSLG) during t_1. Fig. 4d presents a ^{13}C-^{1}H HETCOR spectrum obtained using a short contact time of 200 μs. The short contact time means that predominantly only C-H pairs in close-proximity (i.e., through-bond CH pairs) are observed, and thus the ^{13}C and ^{1}H resonances can be directly assigned. The tilt observed in the cross-peaks is attributed to Anisotropic Bulk Magnetic Susceptibility (ABMS) broadening.[74-75] Table S7 and Table S8 shows a full comparison between experimental ^{1}H isotropic chemical shifts, derived using the ^{13}C-^{1}H HETCOR spectrum shown in Fig. 4d, and calculated GIPAW NMR chemical shift values. The RMSD difference between experiment and calculation for ^{1}H chemical shift values are 0.6 ppm and 0.5 ppm for BIYSEH03 and BIYSEH13 when all hydrogen atoms are considered. These values indicate structural agreement for both models,[11, 76-78] providing further evidence that BIYSEH03, despite its high R-factor, is an accurate structural model.

When comparing different geometry optimisation criteria (full atom versus hydrogens only), the same general trend is noted for ^{1}H σ_{ref} values as was noted for ^{13}C σ_{ref} values: BIYSEH03 magnetic shieldings differ on average by a larger value relative to BIYSEH13 σ_{ref} values, although the effect is reduced relative to ^{13}C. The value of the pyridine ^{1}H GIPAW calculated NMR chemical shifts determined for BIYSEH03 do not significantly vary between the two geometry optimisation cases described. Relative to experimental data, the ^{1}H GIPAW NMR shift of H17 calculated from the hydrogen-only geometry-optimised BIYSEH03

structural model differs by 0.9 ppm compared to experiment, as opposed to 0.5 ppm for a full atom geometry optimisation (see H17 values in Table S7). This appears to agree with the observation that the largest proton displacement extracted from the structural models was H17 (see Table S2).

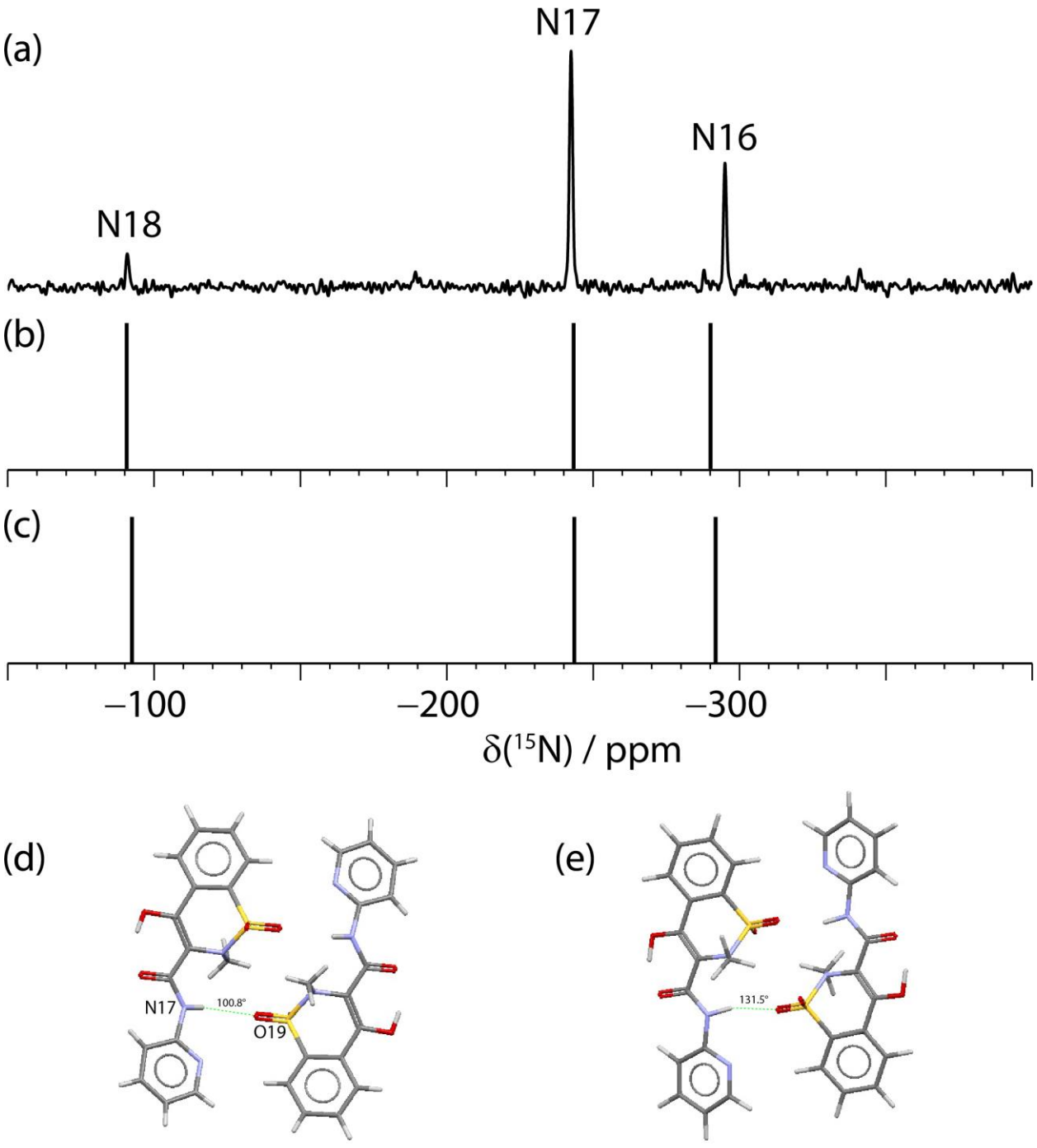

Figure 5. (a) A ^{15}N CPMAS spectrum obtained for β-piroxicam at 11.7 T and a MAS frequency of 10 kHz. (b, c) Stick spectra representing calculated ^{15}N chemical shift GIPAW NMR values calculated for the (b) BIYSEH03 and (c) BIYSEH13 geometry optimised crystal structures. To convert to a scale comparable to liquid nitromethane at 0

ppm, $\delta_{iso} = -(\sigma_{iso} - \sigma_{ref})$, where $\sigma_{ref} = -160.1$ ppm (BIYSEH03) and -161.1 ppm (BIYSEH13). σ_{ref} was calculated from averaging the $\delta(^{15}N)_{expt}$ and σ_{iso} values. (d, e) Extracts of the BIYSEH03 structural model showing putative N17-H17…O19 interactions (d) before and (e) after geometry optimisation.

Fig. 5 compares ^{15}N experimental chemical shifts and calculated GIPAW NMR chemical shifts. As for ^{13}C and ^{1}H, there is good agreement between chemical shift values for both structural models. It is noted that for the case of the putative intermolecular hydrogen bond,[79] N17-H17…O19, bond distances and angles changed significantly in BIYSEH03 after geometry optimisation, as is presented in Fig 5, parts (d, e). As N17 directly participates in this interaction, the absence of a significant difference between the ^{15}N experimental chemical shifts relative to the calculated GIPAW NMR chemical shift values indicates that both structures are correct after geometry optimisation.

Further insight into intermolecular packing in the structural model can be obtained from the comparison of chemical shifts calculated for the full crystal relative to those in an isolated molecule. To simulate an isolated molecule in a GIPAW calculation, a molecule is taken from the related crystal structure and placed in a vacuum supercell, i.e. a unit cell with sufficiently large lattice parameters to effectively remove any intermolecular interactions between neighbouring molecules.[24, 32] Any protons participating in strong hydrogen bonding are no longer deshielded for an isolated molecule calculation, and therefore have a lower ppm value, whereas chemical shifts of protons subject to the effects of a ring current increase in the isolated molecule calculation relative to a full crystal. From inspection of Table 2, H5, H12 and H21 produce significant (magnitude greater than 1 ppm) chemical shift differences between the isolated molecule and the full crystal. H5 and H12 are aromatic protons, and therefore the change in chemical shift for an isolated molecule calculation is attributed to the absence of ring currents associated with aromatic moieties, whereby aromatic dispersive forces are responsible for driving the intermolecular arrangement, that are otherwise present in the full crystal. Interestingly, H17 does not display any significant change in proton chemical shift, showing that this does not participate in an intermolecular hydrogen bond, which is unsurprising from inspection of the non-planar extracted N17-H17…O19 bond angle. Table S4 in the supporting information describes the N17-H17…O19 arrangement for both starting structural models and their respective

geometry-optimised models. Rather, NMR crystallography demonstrates that intermolecular packing arrangement for both structural models is predominately driven by aromatic dispersive forces, as opposed to a N17-H17…O19 hydrogen bonding motif.

Table 2. GIPAW NMR calculated ^{1}H chemical shifts for a full crystal and for an isolated molecule in a vacuum for β-piroxicam (BIYSEH03 and 13), together with experimental ^{1}H chemical shifts.

		BIYSEH03			**BIYSEH13**		
Site	$\delta(^{1}H)_{expt}$ / ppm	$\delta(^{1}H)_{calc}$ / ppm Full crystal	$\delta(^{1}H)_{calc}$ /ppm Single molecule [a]	Difference / ppm	$\delta(^{1}H)_{calc}$ / ppm Full crystal	$\delta(^{1}H)_{calc}$ / ppm Single molecule [a]	Difference / ppm
H2	7.8	7.4	7.6	–0.2	7.4	7.6	–0.2
H3	7.4	7.4	7.4	0.0	7.4	7.4	0.0
H4	7.7	7.6	7.4	0.2	7.6	7.4	0.2
H5	6.4	6.1	8.0	–1.9	6.1	7.9	–1.8
H10a	3.2	3.5	3.2	0.3	3.4	3.3	0.1
H10b	3.2	2.6	2.2	0.4	2.4	2.2	0.3
H10c	3.2	3.6	2.8	0.8	3.8	2.8	1.0
H12	6.4	6.3	8.5	–2.2	6.2	8.4	–2.2
H13	6.6	6.8	7.6	–0.8	6.9	7.6	–0.7
H14	6.8	6.4	6.8	–0.4	6.4	6.8	–0.4
H15	8.3	8.2	8.2	0.0	8.1	8.2	–0.1
H17	9.6	9.2	9.0	0.2	9.3	9.0	0.3
H21	12.4	14.0	15.5	–1.5	13.6	15.3	–1.7

[a] The same σ_{ref} values were used as specified in Fig. 4.

Using 2D MAS NMR to verify extracted intermolecular proximities from geometry-optimised structural models

An important confirmation of the intermolecular packing arrangement of the structural models is obtained from comparison between intermolecular correlations observed in 2D MAS NMR spectra relative to extracted intermolecular distances from the geometry-optimised structural models. The 2D experiments presented here provide a more qualitative form of structural confirmation. In the following experiments, magnetisation transfer is achieved when a sufficiently strong dipolar coupling between nuclei exists, which is only the case for closer proximity spin-pairs. Consequently, cross-peaks are only observed between nuclei within a proximity of up to approximately 4 Å, although no precise distance measurements are inferred.

Further information concerning the nitrogen environments can be inferred from ^{14}N experiments. ^{14}N is a spin $I = 1$ nucleus, which is typically more experimentally challenging relative to nuclei with $I = 1/2$ owing to the presence of the quadrupolar interaction (see SI for further information).[80-81] While experimental NMR techniques for quadrupolar nuclei are more challenging compared to spin $I = ½$ nuclei, the quadrupolar interaction does provide further information concerning the local electronic environment, and has been demonstrated to be a powerful probe of intermolecular hydrogen bonding.[52, 82-85] Additionally, whereas ^{15}N experiments are severely limited by a low natural abundance (0.4%), ^{14}N has a high abundance (99.6%). In recent years ^{14}N-^{1}H Heteronuclear Multiple Quantum Coherence (HMQC) experiments performed at fast MAS frequencies[52, 83, 86-88] have been demonstrated as a powerful probe of pharmaceuticals.[81, 89] These experiments observe magnetisation upon the more sensitive proton spin, and polarisation is transferred from protons to nitrogen via through-space couplings using a heteronuclear dipolar recoupling scheme. Fast MAS is required to improve resolution in the proton dimension, and to increase the ^{1}H coherence lifetime during the application of *rf* recoupling.[86, 90]

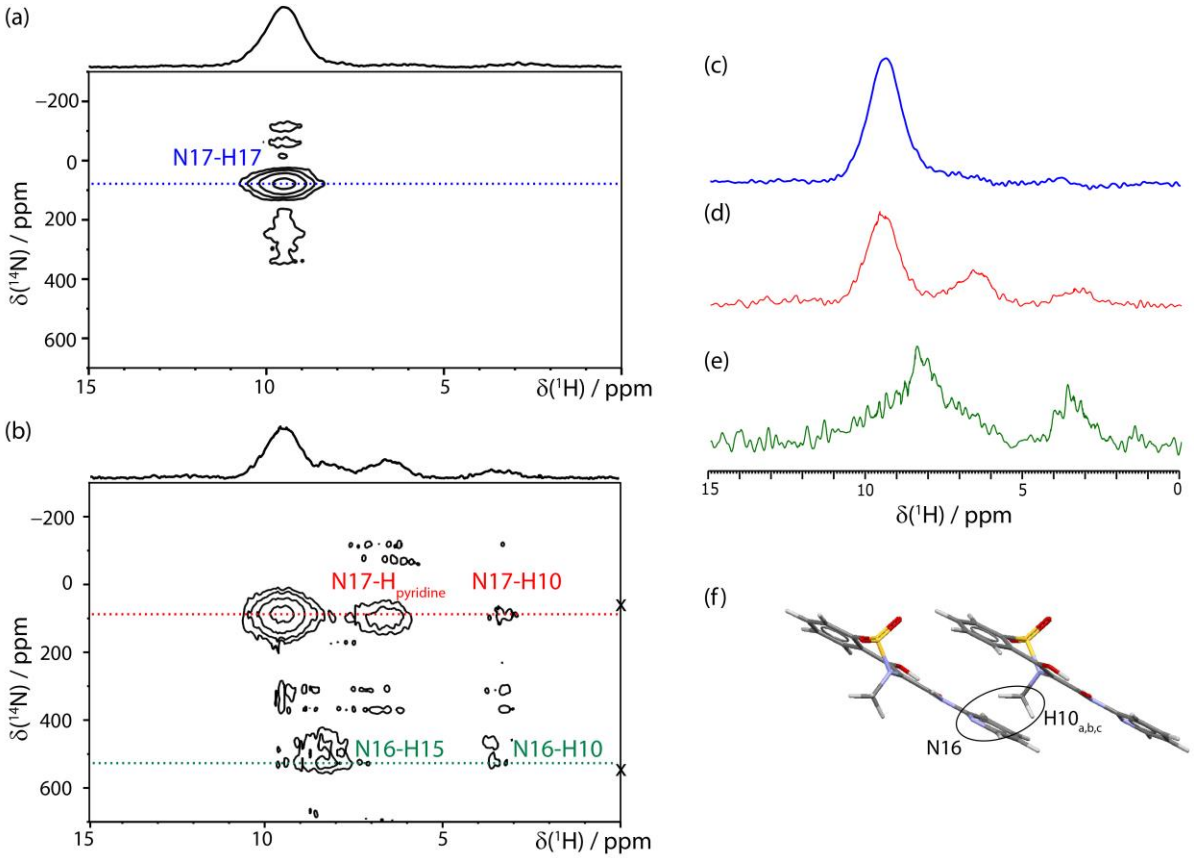

Figure 6. (a, b) 2D ^{14}N-^{1}H HMQC spectra with ^{1}H skyline projections of β-piroxicam (ν_r = 60 kHz, B_0 = 16.4 T) using n = 2 rotary resonance recoupling of ^{14}N-^{1}H heteronuclear dipolar couplings for (a) τ_{RCPL} = 266.7 μs and (b) τ_{RCPL} = 533.3 μs. The crosses indicate the predicted centre-of-gravity of the N16 and N17 resonances determined from GIPAW NMR calculations. (c, d, e) ^{1}H individual sub-spectra taken through the ^{14}N resonance of corresponding colour to demonstrate which ^{14}N-^{1}H heteronuclear dipolar couplings are recoupled owing to close through-space proximity. (f) Stacking arrangement of β-piroxicam from the geometry-optimised BIYSEH03 structural model.

In Fig. 6, ^{14}N-^{1}H HMQC spectra recorded with different recoupling times are presented. These spectra were obtained at B_0 = 16.4 T. Spectra obtained at 9.4 T can be found in the supporting information (Fig. S6). Only the N17 site, which has the smallest C_Q, is visible at lower field, whereas N-H correlations between N16 and neighbouring protons are also visible at 16.4 T. Extracted distances referred to herein include hydrogen positions as hydrogen directly participates in the experimental observations shown.

At short recoupling times, only the directly-bonded NH correlation is observed, see Fig. 6a. A slice of the proton dimension, taken through the isotropic shift of N17 shows a single peak corresponding to the NH proton (H17), Fig. 6c. At longer recoupling times, see Fig. 6b, longer-range N-H proximities are visible.[86]

A slice taken through N17 for a longer recoupling time is presented in Fig. 6d, and the intramolecular correlations are labelled accordingly in Fig. 6b. Correlations from N16 to methyl protons and a further correlation to a resonance at approximately 8.3 ppm are visible in Fig. 6e. The N16 correlation to the methyl protons must be an intermolecular correlation; inspection of the geometry optimised structural model shows the closest intramolecular N16-methyl distance is approximately 4.3 Å, whereas the shortest N16-H10 intermolecular distance is 3.1 Å. In Fig. 6f, an extract from the geometry optimised BIYSEH03 structural model shows the stacking arrangement between molecules, with this methyl-N16 proximity circled.

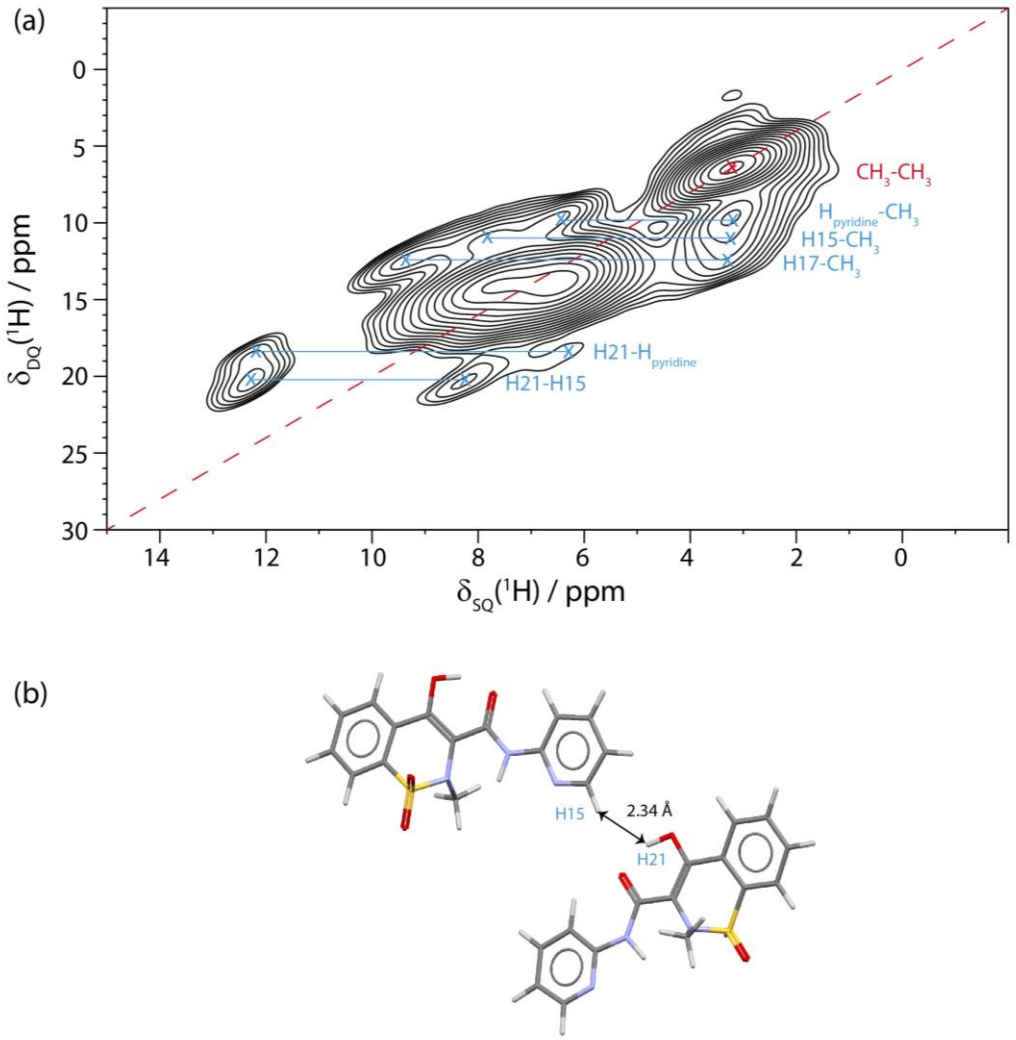

Figure 7. (a) A ^{1}H DQ-SQ MAS spectrum of β-piroxicam recorded at ν_r = 60 kHz and $\nu_0(^1H)$ = 400 MHz using one rotor period of Back-to-Back dipolar recoupling. The diagonal red line at $\delta_{DQ} = 2\delta_{SQ}$ is included as a visual aid, and

connected cross-peaks are indicated by blue horizontal dashed lines. (b) Structural extract from BIYSEH03 highlighting the close proximity (2.34 Å) of H15 and H21 as a consequence of the intermolecular packing arrangement.

Further details of through-space correlations that can be directly linked to the geometry optimised structural model are determinable from a ^{1}H-^{1}H DQ MAS experiment[91-92] using BABA recoupling.[46-47, 91] Performed at fast MAS to improve spectral resolution, the homonuclear dipolar coupling is selectively recoupled during the DQ excitation and reconversion periods. Consequently, correlations between close-proximity through-space protons produce a pair of peaks (connected by blue dashed lines in Fig. 7) horizontally equidistant from a diagonal line $\delta_{DQ} = 2\delta_{SQ}$ (included as a visual aid in red). Cross peaks on the diagonal correspond to protons close enough in space to produce a through-space correlation to the same proton in a neighbouring molecule, or a neighbouring proton with the same chemical shift value, e.g. the on-diagonal peak for the methyl protons.[92]

A clear cross peak between H21 (OH proton at 12.4 ppm) and H15 (at 8.3 ppm) is visible in Fig. 7a. As H21 and H15 are the only proton resonances at these chemical shift values then this cross-peak can be assigned with confidence. Inspection of the geometry optimised structural model (see Fig. 7b) indicates that this corresponds to an intermolecular distance of approximately 2.4 Å (the intramolecular distance between H21 and H15 is 7.7 Å). A cross-peak between H21 and a resonance at 6.4 ppm is also visible. This is potentially an intermolecular correlation to a neighbouring pyridine proton, H14, although owing to overlapping proton resonances in this spectral region this assignment is not unambiguous. A cross-peak between H17 at 9.6 ppm and methyl protons at 3.2 ppm is observed, which is consistent with the correlation between N17 are the methyl protons in the ^{14}N-^{1}H HMQC experiment (see Fig. 6d).

Conclusions

We have demonstrated that NMR crystallography can act as a valuable complementary tool to diffraction studies and associated metrics, such as the R-factor, to build confidence for two structural models solved for β-piroxicam using PXRD and SCXRD, respectively. In particular the structure solution solved from PXRD, BIYSEH03, has a high R-factor and therefore any associated solid-state risk assessment performed

for this model, or a model with an equivalently high R-factor, would benefit from any methodology that increases confidence in the model, especially when the only structural model available has been solved using PXRD.

We observe a convergence between the two structure solutions after geometry optimisation, which both give good agreement between calculated and experimental NMR parameters, and are therefore demonstrably more accurate structural models of β-piroxicam, relative to both starting structures. The change in atomic positions after a geometry optimisation step clearly demonstrates the value in performing a geometry optimisation as a routine step in any diffraction solved structural model,[64] particularly for a powder diffraction. The results herein also indicate that in most cases all atoms in organic materials should be relaxed during a geometry optimisation,[93] at least for a structural model solved using PXRD data. Herein, this was demonstrated by the deviation in N17 and the pyridine ring between full-atom and hydrogen only geometry optimisation. We demonstrate that NMR crystallography is a valuable tool for the verification of different crystal structure solutions and as an additional indicator of the accuracy of a proposed structural model to be used in conjunction with the existing R-factor.

Agreement between experimental chemical shifts and calculated GIPAW NMR chemical shifts determined for ^{13}C, ^{1}H and ^{15}N verifies this convergence. The two structure solutions have the same GIPAW NMR chemical shift values within reasonable error, and crucially both have a broad agreement with experiment. Additional insight into the intermolecular arrangement of β-piroxicam is evident from comparison between full crystal and isolated molecule calculations. These demonstrate that the intermolecular packing arrangement of both models, which we consider accurate from chemical shift comparisons detailed, is predominately via aromatic dispersive forces, as opposed to intermolecular hydrogen bonding. Furthermore, we also note that experimentally observed intermolecular correlations in ^{1}H DQ and ^{14}N-^{1}H MAS NMR spectra between close-proximity spin-pairs agree with predicted short-range intermolecular proximities extracted for both structural models, which provides further evidence of the accuracy of both structural models.

Associated Content

The calculated and experimental data for this study are provided as a supporting dataset from WRAP, the Warwick Research Archive Portal at http://wrap.warwick.ac.uk/***. The supporting information (PDF) contains: (i) experimental verification of β-piroxicam form using PXRD, (ii) atomic displacement tables, (iii) comparison of geometry optimised structures of BIYSEH03 and BIYSEH13, (iv) a ^{13}C CP non-quaternary suppression spectrum, (v) a ^{13}C-^{1}H HETCOR spectrum obtained with a longer contact time, (vi) tables comparing experimental and calculated NMR parameters, and (vii) ^{14}N-^{1}H spectra obtained at B_0 = 9.4 T. Geometry optimised structural models (cif format) of BIYSEH03 and BIYSEH13 calculated with different relaxation conditions are also available to freely download.

Acknowledgements

We acknowledge support from the Collaborative Computing Project for NMR Crystallography (CCP-NC) funded by EPSRC (EP/M022501/1). PH acknowledges support from EPSRC grant EP/L012243/1. The European Research Council (ERC Starting Grant 639907 awarded to Jozef Lewandowski) and the University of Warwick funded the 700 MHz Bruker Avance III spectrometer used for ^{14}N-^{1}H experiments. We acknowledge assistance from Anjali Menakath with the recording of the ^{14}N-^{1}H spectra (700 MHz).

References

(1) Feeder, N.; Pidcock, E.; Reilly, A. M.; Sadiq, G.; Doherty, C. L.; Back, K. R.; Meenan, P.; Docherty, R., The integration of solid-form informatics into solid-form selection. *J. Pharm. Pharmacol.* **2015,** *67*, 857-868.

(2) Hughes, C. E.; Reddy, G. N. M.; Masiero, S.; Brown, S. P.; Williams, P. A.; Harris, K. D. M., Determination of a complex crystal structure in the absence of single crystals: analysis of powder X-ray diffraction data, guided by solid-state NMR and periodic DFT calculations, reveals a new 2'-deoxyguanosine structural motif. *Chem. Sci.* **2017,** *8*, 3971-3979.

(3) Flack, H., On enantiomorph-polarity estimation. *Acta Crystallogr. Sect. A: Found. Crystallogr.* **1983,** *39*, 876-881.

(4) Flack, H. D.; Bernardinelli, G., Reporting and evaluating absolute-structure and absolute-configuration determinations. *J. Appl. Crystallogr.* **2000,** *33*, 1143-1148.

(5) Toby, B. H., R factors in Rietveld analysis: How good is good enough? *Powder Diffr.* **2012,** *21*, 67-70.

(6) Groom, C. R.; Bruno, I. J.; Lightfoot, M. P.; Ward, S. C., The Cambridge Structural Database. *Acta Crystallogr. Sect. B: Struct. Sci.* **2016,** *72*, 171-179.

(7) Buchsbaum, C.; Schmidt, M. U., Rietveld refinement of a wrong crystal structure. *Acta Crystallogr. Sect. B: Struct. Sci.* **2007,** *63*, 926-932.
(8) Harris, R. K., NMR crystallography: the use of chemical shifts. *Solid State Sci.* **2004,** *6*, 1025-1037.
(9) Elena, B.; Pintacuda, G.; Mifsud, N.; Emsley, L., Molecular Structure Determination in Powders by NMR Crystallography from Proton Spin Diffusion. *J. Am. Chem. Soc.* **2006,** *128*, 9555-9560.
(10) Taulelle, F., Fundamental Principles of NMR Crystallography. In *eMagRes*, John Wiley & Sons, Ltd: 2007.
(11) Salager, E.; Stein, R. S.; Pickard, C. J.; Elena, B.; Emsley, L., Powder NMR crystallography of thymol. *Phys. Chem. Chem. Phys.* **2009,** *11*, 2610-2621.
(12) Bonhomme, C.; Gervais, C.; Babonneau, F.; Coelho, C.; Pourpoint, F.; Azaïs, T.; Ashbrook, S. E.; Griffin, J. M.; Yates, J. R.; Mauri, F.; Pickard, C. J., First-Principles Calculation of NMR Parameters Using the Gauge Including Projector Augmented Wave Method: A Chemist's Point of View. *Chem. Rev.* **2012,** *112*, 5733-5779.
(13) Ashbrook, S. E.; McKay, D., Combining solid-state NMR spectroscopy with first-principles calculations - a guide to NMR crystallography. *Chem. Commun.* **2016,** *52*, 7186-7204.
(14) Bryce, D., NMR crystallography: structure and properties of materials from solid-state nuclear magnetic resonance observables. *IUCrJ* **2017,** *4*, 350-359.
(15) Namespetra, A. M.; Hirsh, D. A.; Hildebrand, M. P.; Sandre, A. R.; Hamaed, H.; Rawson, J. M.; Schurko, R. W., ^{35}Cl solid-state NMR spectroscopy of HCl pharmaceuticals and their polymorphs in bulk and dosage forms. *CrystEngComm* **2016,** *18*, 6213-6232.
(16) Abraham, A.; Apperley, D. C.; Byard, S. J.; Ilott, A. J.; Robbins, A. J.; Zorin, V.; Harris, R. K.; Hodgkinson, P., Characterising the role of water in sildenafil citrate by NMR crystallography. *CrystEngComm* **2016,** *18*, 1054-1063.
(17) Chierotti, M. R.; Gobetto, R., NMR crystallography: the use of dipolar interactions in polymorph and co-crystal investigation. *CrystEngComm* **2013,** *15*, 8599-8612.
(18) Fernandes, J. A.; Sardo, M.; Mafra, L.; Choquesillo-Lazarte, D.; Masciocchi, N., X-ray and NMR Crystallography Studies of Novel Theophylline Cocrystals Prepared by Liquid Assisted Grinding. *Cryst. Growth Des.* **2015,** *15*, 3674-3683.
(19) Luedeker, D.; Gossmann, R.; Langer, K.; Brunklaus, G., Crystal Engineering of Pharmaceutical Co-crystals: "NMR Crystallography" of Niclosamide Co-crystals. *Cryst. Growth Des.* **2016,** *16*, 3087-3100.
(20) Kerr, H. E.; Softley, L. K.; Suresh, K.; Hodgkinson, P.; Evans, I. R., Structure and physicochemical characterization of a naproxen-picolinamide cocrystal. *Acta Crystallogr. Sect. C: Cryst. Struct. Commun.* **2017,** *73*, 168-175.
(21) Mafra, L.; Santos, S. M.; Siegel, R.; Alves, I.; Almeida Paz, F. A.; Dudenko, D.; Spiess, H. W., Packing Interactions in Hydrated and Anhydrous Forms of the Antibiotic Ciprofloxacin: a Solid-State NMR, X-ray Diffraction, and Computer Simulation Study. *J. Am. Chem. Soc.* **2012,** *134*, 71-74.
(22) Reddy, G. N. M.; Cook, D. S.; Iuga, D.; Walton, R. I.; Marsh, A.; Brown, S. P., An NMR crystallography study of the hemihydrate of 2', 3'-O-isopropylidineguanosine. *Solid State Nucl. Magn. Reson.* **2015,** *65*, 41-48.
(23) Watts, A. E.; Maruyoshi, K.; Hughes, C. E.; Brown, S. P.; Harris, K. D. M., Combining the Advantages of Powder X-ray Diffraction and NMR Crystallography in Structure Determination of the Pharmaceutical Material Cimetidine Hydrochloride. *Cryst. Growth Des.* **2016,** *16*, 1798-1804.
(24) Zilka, M.; Sturniolo, S.; Brown, S. P.; Yates, J. R., Visualising crystal packing interactions in solid-state NMR: Concepts and applications. *J. Chem. Phys.* **2017,** *147*, 144203.
(25) Perras, F. A.; Bryce, D. L., Multinuclear Magnetic Resonance Crystallographic Structure Refinement and Cross-Validation Using Experimental and Computed Electric Field Gradients: Application to $Na_2Al_2B_2O_7$. *J. Phys. Chem. C* **2012,** *116*, 19472-19482.
(26) Romao, C. P.; Perras, F. A.; Werner-Zwanziger, U.; Lussier, J. A.; Miller, K. J.; Calahoo, C. M.; Zwanziger, J. W.; Bieringer, M.; Marinkovic, B. A.; Bryce, D. L.; White, M. A., Zero Thermal Expansion in $ZrMgMo_3O_{12}$: NMR Crystallography Reveals Origins of Thermoelastic Properties. *Chem. Mater.* **2015,** *27*, 2633-2646.

(27) Holmes, S. T.; Schurko, R. W., Refining Crystal Structures with Quadrupolar NMR and Dispersion-Corrected Density Functional Theory. *J. Phys. Chem. C* **2018,** *122*, 1809-1820.
(28) Dudenko, D. V.; Yates, J. R.; Harris, K. D. M.; Brown, S. P., An NMR crystallography DFT-D approach to analyse the role of intermolecular hydrogen bonding and π-π interactions in driving cocrystallisation of indomethacin and nicotinamide. *CrystEngComm* **2013,** *15*, 8797-8807.
(29) Bradley, J. P.; Velaga, S. P.; Antzutkin, O. N.; Brown, S. P., Probing Intermolecular Crystal Packing in γ-Indomethacin by High-Resolution ^{1}H Solid-State NMR Spectroscopy. *Cryst. Growth Des.* **2011,** *11*, 3463-3471.
(30) Filip, X.; Grosu, I.-G.; Miclaus, M.; Filip, C., NMR crystallography methods to probe complex hydrogen bonding networks: application to structure elucidation of anhydrous quercetin. *CrystEngComm* **2013,** *15*, 4131-4142.
(31) Carignani, E.; Borsacchi, S.; Bradley, J. P.; Brown, S. P.; Geppi, M., Strong Intermolecular Ring Current Influence on ^{1}H Chemical Shifts in Two Crystalline Forms of Naproxen: a Combined Solid-State NMR and DFT Study. *J. Phys. Chem. C* **2013,** *117*, 17731-17740.
(32) Yates, J. R.; Pham, T. N.; Pickard, C. J.; Mauri, F.; Amado, A. M.; Gil, A. M.; Brown, S. P., An Investigation of Weak CH···O Hydrogen Bonds in Maltose Anomers by a Combination of Calculation and Experimental Solid-State NMR Spectroscopy. *J. Am. Chem. Soc.* **2005,** *127*, 10216-10220.
(33) Brogden, R. N.; Heel, R. C.; Speight, T. M.; Avery, G. S., Piroxicam: A Review of its Pharmacological Properties and Therapeutic Efficacy. *Drugs* **1981,** *22*, 165-187.
(34) Sheth, A. R.; Bates, S.; Muller, F. X.; Grant, D. J. W., Polymorphism in Piroxicam. *Cryst. Growth Des.* **2004,** *4*, 1091-1098.
(35) Shi, X.; El Hassan, N.; Ikni, A.; Li, W.; Guiblin, N.; Spasojevic de-Bire, A.; Ghermani, N. E., Experimental electron densities of neutral and zwitterionic forms of the drug piroxicam. *CrystEngComm* **2016,** *18*, 3289-3299.
(36) Sheth, A. R.; Bates, S.; Muller, F. X.; Grant, D. J. W., Local Structure in Amorphous Phases of Piroxicam from Powder X-ray Diffractometry. *Cryst. Growth Des.* **2005,** *5*, 571-578.
(37) Clark, S. J.; Segall, M. D.; Pickard, C. J.; Hasnip, P. J.; Probert, M. I. J.; Refson, K.; Payne, M. C., First principles methods using CASTEP. *Z. Kristallogr.* **2005,** *220*, 567.
(38) Pickard, C. J.; Mauri, F., All-electron magnetic response with pseudopotentials: NMR chemical shifts. *Phys. Rev. B* **2001,** *63*, 245101.
(39) Yates, J. R.; Pickard, C. J.; Mauri, F., Calculation of NMR chemical shifts for extended systems using ultrasoft pseudopotentials. *Phys. Rev. B* **2007,** *76*, 024401.
(40) Metz, G.; Wu, X. L.; Smith, S. O., Ramped-Amplitude Cross Polarization in Magic-Angle-Spinning NMR. *J. Magn. Reson., Ser A* **1994,** *110*, 219-227.
(41) van Rossum, B. J.; Förster, H.; de Groot, H. J. M., High-Field and High-Speed CP-MAS ^{13}C NMR Heteronuclear Dipolar-Correlation Spectroscopy of Solids with Frequency-Switched Lee–Goldburg Homonuclear Decoupling. *J. Magn. Reson.* **1997,** *124*, 516-519.
(42) Khitrin, A.; Fung, B. M., Design of heteronuclear decoupling sequences for solids. *J. Chem. Phys.* **2000,** *112*, 2392-2398.
(43) Fung, B. M.; Khitrin, A. K.; Ermolaev, K., An Improved Broadband Decoupling Sequence for Liquid Crystals and Solids. *J. Magn. Reson.* **2000,** *142*, 97-101.
(44) Bielecki, A.; Kolbert, A. C.; Levitt, M. H., Frequency-switched pulse sequences: Homonuclear decoupling and dilute spin NMR in solids. *Chem. Phys. Lett.* **1989,** *155*, 341-346.
(45) Morcombe, C. R.; Zilm, K. W., Chemical shift referencing in MAS solid state NMR. *J. Magn. Reson.* **2003,** *162*, 479-486.
(46) Sommer, W.; Gottwald, J.; Demco, D. E.; Spiess, H. W., Dipolar Heteronuclear Multiple-Quantum NMR Spectroscopy in Rotating Solids. *J. Magn. Reson., Ser A* **1995,** *113*, 131-134.
(47) Schnell, I.; Lupulescu, A.; Hafner, S.; Demco, D. E.; Spiess, H. W., Resolution Enhancement in Multiple-Quantum MAS NMR Spectroscopy. *J. Magn. Reson.* **1998,** *133*, 61-69.
(48) Hayashi, S.; Hayamizu, K., Chemical Shift Standards in High-Resolution Solid-State NMR (1) ^{13}C, ^{29}Si, and ^{1}H Nuclei. *Bull. Chem. Soc. Jpn.* **1991,** *64*, 685-687.

(49) Hayashi, S.; Hayamizu, K., Chemical Shift Standards in High-Resolution Solid-State NMR (2) ^{15}N Nuclei. *Bull. Chem. Soc. Jpn.* **1991,** *64*, 688-690.
(50) Harris, R. K.; Becker, E. D.; De Menezes, S. M. C.; Granger, P.; Hoffman, R. E.; Zilm, K. W., Further Conventions for NMR Shielding and Chemical Shifts (IUPAC Recommendations 2008). *Magn. Reson. Chem.* **2008,** *46*, 582-598.
(51) Martin, G. E.; Hadden, C. E., Long-Range ^{1}H−^{15}N Heteronuclear Shift Correlation at Natural Abundance. *J. Nat. Prod.* **2000,** *63*, 543-585.
(52) Gan, Z.; Amoureux, J. P.; Trébosc, J., Proton-detected ^{14}N MAS NMR using homonuclear decoupled rotary resonance. *Chem. Phys. Lett.* **2007,** *435*, 163-169.
(53) Oas, T. G.; Griffin, R. G.; Levitt, M. H., Rotary resonance recoupling of dipolar interactions in solid‐state nuclear magnetic resonance spectroscopy. *J. Chem. Phys.* **1988,** *89*, 692-695.
(54) Costa, P. R.; Gross, J. D.; Hong, M.; Griffin, R. G., Solid-state NMR measurement of Ψ in peptides: a NCCN 2Q-heteronuclear local field experiment. *Chem. Phys. Lett.* **1997,** *280*, 95-103.
(55) Webber, A. L.; Masiero, S.; Pieraccini, S.; Burley, J. C.; Tatton, A. S.; Iuga, D.; Pham, T. N.; Spada, G. P.; Brown, S. P., Identifying Guanosine Self Assembly at Natural Isotopic Abundance by High-Resolution ^{1}H and ^{13}C Solid-State NMR Spectroscopy. *J. Am. Chem. Soc.* **2011,** *133*, 19777-19795.
(56) Perdew, J. P.; Burke, K.; Ernzerhof, M., Generalized Gradient Approximation Made Simple. *Phys. Rev. Lett.* **1996,** *77*, 3865-3868.
(57) Tkatchenko, A.; Scheffler, M., Accurate Molecular Van Der Waals Interactions from Ground-State Electron Density and Free-Atom Reference Data. *Phys. Rev. Lett.* **2009,** *102*, 073005.
(58) Sturniolo, S.; Green, T. F. G.; Hanson, R. M.; Zilka, M.; Refson, K.; Hodgkinson, P.; Brown, S. P.; Yates, J. R., Visualization and processing of computed solid-state NMR parameters: MagresView and MagresPython. *Solid State Nucl. Magn. Reson.* **2016,** *78*, 64-70.
(59) Sheth, A. R.; Lubach, J. W.; Munson, E. J.; Muller, F. X.; Grant, D. J. W., Mechanochromism of Piroxicam Accompanied by Intermolecular Proton Transfer Probed by Spectroscopic Methods and Solid-Phase Changes. *J. Am. Chem. Soc.* **2005,** *127*, 6641-6651.
(60) Kojic-Prodic, B.; Ruzic-Toros, Z., Structure of the anti-inflammatory drug 4-hydroxy-2-methyl-N-2-pyridyl-2H-1λ6,2-benzothiazine-3-carboxamide 1,1-dioxide (piroxicam). *Acta Crystallogr. Sect. B: Struct. Sci.* **1982,** *38*, 2948-2951.
(61) Taddei, P.; Torreggiani, A.; Simoni, R., Influence of environment on piroxicam polymorphism: Vibrational spectroscopic study. *Biopolymers* **2001,** *62*, 68-78.
(62) Redenti, E.; Zanol, M.; Ventura, P.; Fronza, G.; Comotti, A.; Taddei, P.; Bertoluzza, A., Raman and solid state ^{13}C-NMR investigation of the structure of the 1 : 1 amorphous piroxicam : β-cyclodextrin inclusion compound. *Biospectroscopy* **1999,** *5*, 243-251.
(63) David, W. I. F.; Shankland, K.; van de Streek, J.; Pidcock, E.; Motherwell, W. D. S.; Cole, J. C., DASH: a program for crystal structure determination from powder diffraction data. *J. Appl. Crystallogr.* **2006,** *39*, 910-915.
(64) van de Streek, J.; Neumann, M. A., Validation of experimental molecular crystal structures with dispersion-corrected density functional theory calculations. *Acta Crystallogr. Sect. B: Struct. Sci.* **2010,** *66*, 544-558.
(65) Vrečer, F.; Vrbinc, M.; Meden, A., Characterization of piroxicam crystal modifications. *Int. J. Pharm.* **2003,** *256*, 3-15.
(66) Vogt, F. G.; Clawson, J. S.; Strohmeier, M.; Edwards, A. J.; Pham, T. N.; Watson, S. A., Solid-State NMR Analysis of Organic Cocrystals and Complexes. *Cryst. Growth Des.* **2009,** *9*, 921-937.
(67) Liu, W.; Wang, W. D.; Wang, W.; Bai, S.; Dybowski, C., Influence of Structure on the Spectroscopic Properties of the Polymorphs of Piroxicam. *J. Phys. Chem. B* **2010,** *114*, 16641-16649.
(68) Dračínský, M.; Hodgkinson, P., Effects of Quantum Nuclear Delocalisation on NMR Parameters from Path Integral Molecular Dynamics. *Chem. Eur. J.* **2014,** *20*, 2201-2207.
(69) Bryce, D. L.; Bultz, E. B.; Aebi, D., Calcium-43 Chemical Shift Tensors as Probes of Calcium Binding Environments. Insight into the Structure of the Vaterite $CaCO_3$ Polymorph by ^{43}Ca Solid-State NMR Spectroscopy. *J. Am. Chem. Soc.* **2008,** *130*, 9282-9292.

(70) Gervais, C.; Jones, C.; Bonhomme, C.; Laurencin, D., Insight into the local environment of magnesium and calcium in low-coordination-number organo-complexes using ^{25}Mg and ^{43}Ca solid-state NMR: a DFT study. *Acta Crystallogr. Sect. C: Cryst. Struct. Commun.* **2017,** *73*, 208-218.
(71) Burgess, K. M. N.; Korobkov, I.; Bryce, D. L., A Combined Solid-State NMR and X-ray Crystallography Study of the Bromide Ion Environments in Triphenylphosphonium Bromides. *Chem. Eur. J.* **2012,** *18*, 5748-5758.
(72) Li, X.; Tapmeyer, L.; Bolte, M.; van de Streek, J., Crystallographic and Dynamic Aspects of Solid-State NMR Calibration Compounds: Towards ab Initio NMR Crystallography. *ChemPhysChem* **2016,** *17*, 2496-2502.
(73) Webber, A. L.; Emsley, L.; Claramunt, R. M.; Brown, S. P., NMR Crystallography of Campho[2,3-c]pyrazole (Z' = 6): Combining High-Resolution ^{1}H-^{13}C Solid-State MAS NMR Spectroscopy and GIPAW Chemical-Shift Calculations. *J. Phys. Chem. A* **2010,** *114*, 10435-10442.
(74) Harris, R. K.; Hodgkinson, P.; Zorin, V.; Dumez, J.-N.; Elena-Herrmann, B.; Emsley, L.; Salager, E.; Stein, R. S., Computation and NMR crystallography of terbutaline sulfate. *Magn. Reson. Chem.* **2010,** *48*, S103-S112.
(75) Hanrahan, M. P.; Venkatesh, A.; Carnahan, S. L.; Calahan, J. L.; Lubach, J. W.; Munson, E. J.; Rossini, A. J., Enhancing the Resolution of ^{1}H and ^{13}C Solid-State NMR Spectra by Reduction of Anisotropic Bulk Magnetic Susceptibility Broadening. *Phys. Chem. Chem. Phys.* **2017,** *19*, 28153-28162.
(76) Salager, E.; Day, G. M.; Stein, R. S.; Pickard, C. J.; Elena, B.; Emsley, L., Powder Crystallography by Combined Crystal Structure Prediction and High-Resolution ^{1}H Solid-State NMR Spectroscopy. *J. Am. Chem. Soc.* **2010,** *132*, 2564-2566.
(77) Widdifield, C. M.; Robson, H.; Hodgkinson, P., Furosemide's one little hydrogen atom: NMR crystallography structure verification of powdered molecular organics. *Chem. Commun.* **2016,** *52*, 6685-6688.
(78) Widdifield, C. M.; Nilsson Lill, S. O.; Broo, A.; Lindkvist, M.; Pettersen, A.; Svensk Ankarberg, A.; Aldred, P.; Schantz, S.; Emsley, L., Does Z' equal 1 or 2? Enhanced powder NMR crystallography verification of a disordered room temperature crystal structure of a p38 inhibitor for chronic obstructive pulmonary disease. *Phys. Chem. Chem. Phys.* **2017,** *19*, 16650-16661.
(79) Wood, P. A.; Allen, F. H.; Pidcock, E., Hydrogen-bond directionality at the donor H atom-analysis of interaction energies and database statistics. *CrystEngComm* **2009,** *11*, 1563-1571.
(80) Samoson, A., Satellite transition high-resolution NMR of quadrupolar nuclei in powders. *Chem. Phys. Lett.* **1985,** *119*, 29-32.
(81) Tatton, A. S.; Pham, T. N.; Vogt, F. G.; Iuga, D.; Edwards, A. J.; Brown, S. P., Probing intermolecular interactions and nitrogen protonation in pharmaceuticals by novel ^{15}N-edited and 2D ^{14}N-^{1}H solid-state NMR. *CrystEngComm* **2012,** *14*, 2654-2659.
(82) Gervais, C.; Dupree, R.; Pike, K. J.; Bonhomme, C.; Profeta, M.; Pickard, C. J.; Mauri, F., Combined First-Principles Computational and Experimental Multinuclear Solid-State NMR Investigation of Amino Acids. *J. Phys. Chem. A* **2005,** *109*, 6960-6969.
(83) Cavadini, S.; Lupulescu, A.; Antonijevic, S.; Bodenhausen, G., Nitrogen-14 NMR Spectroscopy Using Residual Dipolar Splittings in Solids. *J. Am. Chem. Soc.* **2006,** *128*, 7706-7707.
(84) Kwan, I. C. M.; Mo, X.; Wu, G., Probing Hydrogen Bonding and Ion−Carbonyl Interactions by Solid-State 17O NMR Spectroscopy: G-Ribbon and G-Quartet. *J. Am. Chem. Soc.* **2007,** *129*, 2398-2407.
(85) O'Dell, L. A.; Schurko, R. W., Static solid-state ^{14}N NMR and computational studies of nitrogen EFG tensors in some crystalline amino acids. *Phys. Chem. Chem. Phys.* **2009,** *11*, 7069-7077.
(86) Tatton, A. S.; Bradley, J. P.; Iuga, D.; Brown, S. P., ^{14}N–^{1}H Heteronuclear Multiple-Quantum Correlation Magic-Angle Spinning NMR Spectroscopy of Organic Solids. *Z. Phys. Chem.* **2012,** *226*, 1187.
(87) Cavadini, S.; Abraham, A.; Bodenhausen, G., Proton-detected nitrogen-14 NMR by recoupling of heteronuclear dipolar interactions using symmetry-based sequences. *Chem. Phys. Lett.* **2007,** *445*, 1-5.
(88) Cavadini, S., Indirect detection of nitrogen-14 in solid-state NMR spectroscopy. *Prog. Nucl. Magn. Reson. Sp.* **2010,** *56*, 46-77.

(89) Maruyoshi, K.; Iuga, D.; Antzutkin, O. N.; Alhalaweh, A.; Velaga, S. P.; Brown, S. P., Identifying the intermolecular hydrogen-bonding supramolecular synthons in an indomethacin-nicotinamide cocrystal by solid-state NMR. *Chem. Commun.* **2012,** *48*, 10844-10846.
(90) Nishiyama, Y.; Endo, Y.; Nemoto, T.; Utsumi, H.; Yamauchi, K.; Hioka, K.; Asakura, T., Very fast magic angle spinning ^{1}H-^{14}N 2D solid-state NMR: Sub-micro-liter sample data collection in a few minutes. *J. Magn. Reson.* **2011,** *208*, 44-48.
(91) Geen, H.; Titman, J. J.; Gottwald, J.; Spiess, H. W., Solid-state proton multiple-quantum NMR spectroscopy with fast magic angle spinning. *Chem. Phys. Lett.* **1994,** *227*, 79-86.
(92) Brown, S. P., Applications of high-resolution ^{1}H solid-state NMR. *Solid State Nucl. Magn. Reson.* **2012,** *41*, 1-27.
(93) Harris, R. K.; Hodgkinson, P.; Pickard, C. J.; Yates, J. R.; Zorin, V., Chemical shift computations on a crystallographic basis: some reflections and comments. *Magn. Reson. Chem.* **2007,** *45*, S174-S186.